Conformal Surface Parameterization for Texture Mapping

Steven Haker
Department of Electrical and Computer Engineering
University of Minnesota
Minneapolis, MN 55455

Sigurd Angenent
Department of Mathematics
University of Wisconsin
Madison, Wisconsin 53705

Allen Tannenbaum
Department of Electrical and Computer Engineering
University of Minnesota
Minneapolis, MN 55455

Ron Kikinis
Harvard Medical School
Brigham and Women's Hospital
Harvard University
Boston, MA 02115

Guillermo Sapiro
Department of Electrical and Computer Engineering
University of Minnesota
Minneapolis, MN 55455

Michael Halle
Harvard Medical School
Brigham and Women's Hospital
Harvard University
Boston, MA 02115

March 25, 1999

Report Documentation Page

Form Approved
OMB No. 0704-0188

1. REPORT DATE	2. REPORT TYPE	3. DATES COVERED
25 MAR 1999		**-**

4. TITLE AND SUBTITLE	5a. CONTRACT NUMBER
Conformal Surface Parameterization for Texture Mapping	5b. GRANT NUMBER
	5c. PROGRAM ELEMENT NUMBER
6. AUTHOR(S)	5d. PROJECT NUMBER
	5e. TASK NUMBER
	5f. WORK UNIT NUMBER
7. PERFORMING ORGANIZATION NAME(S) AND ADDRESS(ES) **Air Force Office of Scientific Research (AFOSR),875 North Randolph Street,Suite 325, Room 3112,Arlington,VA,22203-1768**	8. PERFORMING ORGANIZATION REPORT NUMBER
9. SPONSORING/MONITORING AGENCY NAME(S) AND ADDRESS(ES)	10. SPONSOR/MONITOR'S ACRONYM(S)
	11. SPONSOR/MONITOR'S REPORT NUMBER(S)

12. DISTRIBUTION/AVAILABILITY STATEMENT
Approved for public release; distribution unlimited

13. SUPPLEMENTARY NOTES
The original document contains color images.

14. ABSTRACT
see report

15. SUBJECT TERMS

16. SECURITY CLASSIFICATION OF:			17. LIMITATION OF ABSTRACT	18. NUMBER OF PAGES	19a. NAME OF RESPONSIBLE PERSON
a. REPORT	b. ABSTRACT	c. THIS PAGE			
unclassified	**unclassified**	**unclassified**		**19**	

Abstract

In this paper, we give an explicit method for mapping any simply connected surface onto the sphere in a manner which preserves angles. This technique relies on certain conformal mappings from differential geometry. Our method provides a new way to automatically assign texture coordinates to complex undulating surfaces. We demonstrate a finite element method that can be used to apply our mapping technique to a triangulated geometric description of a surface.

1 Introduction

The technique of texture mapping is based on mapping an image either synthesized or digitized onto a given surface. The computer graphics literature has many such works on this topic, e.g., see [12] and the references therein. We will not review all the literature on this subject here, but just some of the key works in order to contrast our approach.

Parameterization of polygonal geometric surfaces has direct use for what Gomes *et al.* refer to as image mapping [13], a category of techniques which includes texture mapping [6] [14] [15], reflection or environment mapping [4], bump mapping [5], and light mapping [20]. As its name implies, image mapping associates a coordinate in image space with every location on the surface of a geometric object. The discrete samples of an image raster addressed by the coordinates in image space are applied to the geometric object.

The mathematical basis of this mapping determines whether the image provides the object with the appearance of surface texture, a specular reflection, or some other effect. In this paper, we will focus only on mappings such as texture mapping that are a function of surface location and not those, for example, based on surface orientation.

No matter what kind of image mapping is used, the parameterization function that relates the geometry of the object to image space must be determined. Three rough categories of mapping functions exist [25] [13]. The first is a simple change of coordinates from geometry space to image space. Surface patches and other parametric surfaces, for instance, can often be mapped using their natural parametric coordinate system. The second category, described by Bier and Sloan [3], uses an auxiliary surface as an intermediate between geometry and image. The third category projects the surface onto another surface or geometric solid. For complex non-parameteric objects, finding a usable parameterization function can be a difficult task.

In practice, the techniques used to assign parameters to undulating surfaces are often *ad hoc* and may suffer from distortions, singularities, or other shortcomings.

Several more rigorous techniques have been proposed to parameterize complex surfaces. Bennis *et al.* describe a flattening and cutting technique [2]. More recently, Lee *et al.* have developed a multiresolution approach based on Loop subdivision [18]. Lévy and Mallet use an algorithm for non-distorted mappings for triangle meshes over cuts and other discontinuities [19]. This mapping method combines planar graph theory with penalty functions to preserve right angles. The use of harmonic maps for mapping surfaces with boundary conditions is suggested in [10] for multiresolution analysis of meshes. This approach may have the undesirable property of triangle flipping.

In this paper, we propose a method based on a key fact in conformal geometry. Indeed, one can prove that any surface without holes or self-intersections can be mapped conformally onto the sphere, and any local portion thereof onto a disc. This mapping, called a *conformal equivalence*, is one-to-one, onto, and angle preserving. Moreover, one can explicitly write down how the intrinsic metric on the original surface is transformed and thus areas and the geodesics as well. Specifically, the elements of the first fundamental form (E, F, G) are transformed as $(\rho E, \rho F, \rho G)$ for some positive function ρ depending on the point of the surface. For this reason, conformal mappings are often described as being *similarities in the small*. This means that the mapping can be used to map any planar image or structure on the sphere to our given surface in an angle-preserving manner, and vice versa. *Locally shape is preserved and distances and areas are only changed by a scaling factor.*

We should note that the mapping we construct is bijective (onto and one-to-one), and thus there is no problem with triangles "flipping" or overlapping when mapped to $\mathbf{R}^2$. Further, the method does not require cuts to be made on the surface. The mapping is seamless and thus avoids the problem of blending textures together across cuts.

Besides texture mapping, one may use this technique to find longitude and latitude lines as well as a north and south pole on a given surface S by mapping the corresponding geometric features of the sphere onto S in this conformal manner. Since angles are preserved, the images of the longitudes and latitudes are guaranteed to be orthogonal to each other. Surface deformation and flattening is also very useful for certain problems in medical imaging such as functional magnetic resonance; see [1, 7, 23, 24] and the references therein.

What makes our method practical and easy to implement is the key observation that the conformal transformation may be obtained as the solution of a second order elliptic partial differential equation (PDE) on the surface to be deformed. For triangulated surfaces, there exists a powerful, reliable finite element procedure which can be employed to numerically approximate the conformal mapping function. The heart of this procedure simply involves solving a pair of systems of linear

equations.

We should note that beyond image mapping, the ability to parameterize arbitrary objects of a given topology has a variety of applications. For example, physical properties or other variables can be associated uniquely with locations on a surface.

The outline of this paper is as follows. In Section 2, we sketch the analytical procedure to find the conformal mapping. The details of this are filled in the Appendix of Section 6. In Section 3, we describe how the numerical algorithm works on a triangulated surface. In Section 4, we demonstrate our procedure on some surfaces both synthetic and digitized, and in Section 5 we make some conclusions about further research.

2 Brief Sketch of Mathematical Theory

In this section, we outline the mathematical justification of our surface mapping procedure. See [1] and the Appendix of Section 6 for more details. We start with the basic assumption that the given surface is a topological sphere. This means the surface has no holes, handles, or self-intersections.

Let Σ denote a such a surface in $\mathbf{R}^3$. Let δ_p denote the Dirac delta (impulse) function at $p \in \Sigma$, Δ the Laplace-Beltrami operator on $\Sigma \backslash \{p\}$, and i the square root of -1. (The Laplace-Beltrami operator is the generalization of the usual Laplacian operator to a smooth surface. See [21, 11] and Section 6.) Let S^2 denote the unit sphere in $\mathbf{R}^3$ and let $\mathbf{C}$ be the complex plane. Recall from the Introduction that a conformal equivalence is a one-to-one, onto mapping which preserves angles. We can now state the following result which provides the analytical basis for our texture mapping procedure:

A conformal equivalence $z : \Sigma \backslash \{p\} \to S^2 \backslash \{\text{north pole}\} \cong \mathbf{C}$ may be obtained by solving the equation

$$\Delta z = \left(\frac{\partial}{\partial u} - i \frac{\partial}{\partial v} \right) \delta_p. \tag{1}$$

The derivation of this equation may be found in the Appendix of Section 6. This result means that we can get the conformal equivalence by solving a second order partial differential equation on the surface. Fortunately, on a triangulated surface, this may be carried out using a finite element technique we will describe below. Also, we should note that the equivalence above is unique up to scaling and translation.

3 Finite Element Approximation of Conformal Mapping

We have just sketched the analytical basis for conformally mapping a surface onto a sphere. We want now to describe a numerical procedure for carrying this out. We now assume that Σ is a triangulated surface. We continue to use the notation of the previous section, and let $\sigma = ABC$ be a triangle on whose face the point p lies.

3.1 Finite Element Formulation

We will now briefly outline the finite element method for finding the conformal mapping z which is the solution to the PDE (1). See [16] for details about this method.

First we construct a *weak formulation* of the PDE (1), i.e. we multiply the equation with an arbitrary smooth function f and integrate by parts to get

$$\begin{aligned} \int\int_\Sigma \nabla z \cdot \nabla f dS &= \int\int_\Sigma \left(\frac{\partial}{\partial u} - i\frac{\partial}{\partial v} \right) f \delta_p dS \\ &= \frac{\partial f}{\partial u}(p) - i\frac{\partial f}{\partial v}(p) \end{aligned} \tag{2}$$

where ∇z is the gradient with respect to the induced metric on Σ. One can show that z satisfies (1) if and only if (2) holds for all smooth functions f.

Next, we restrict our attention to the finite dimensional vector space $PL(\Sigma)$ of piecewise linear functions on Σ, and seek a $z \in PL(\Sigma)$ such that (2) holds for all $f \in PL(\Sigma)$. For each vertex $P \in \Sigma$, let ϕ_P be the continuous function such that

$$\begin{cases} \phi_P(P) = 1, \\ \phi_P(Q) = 0, \ Q \neq P, \ Q \text{ a vertex}, \\ \phi_P \text{ is linear on each triangle.} \end{cases} \tag{3}$$

Then these ϕ_P form a basis for $PL(\Sigma)$, and so any $z \in PL(\Sigma)$ can be written as

$$z = \sum_{P \text{ vertex of } \Sigma} z_P \phi_P$$

for some complex numbers z_P. Further, since (2) is linear in f, it is enough to show that (2) holds whenever $f = \phi_Q$ for some Q.

In short, we want to find a vector of complex numbers $z = (z_P)$, containing one element per vertex, such that for all Q,

$$\sum_P z_P \int\int \nabla \phi_P \cdot \nabla \phi_Q dS = \frac{\partial \phi_Q}{\partial u}(p) - i\frac{\partial \phi_Q}{\partial v}(p). \tag{4}$$

3.2 Formulation in Matrix Terms

The formulation (4) is simply a system of linear equations in the complex unknowns z_P.

Let us introduce the real matrix $D = (D_{PQ})$ where

$$D_{PQ} = \int\int \nabla\phi_P \cdot \nabla\phi_Q dS,$$

for each pair of vertices P, Q. It is easy to see that if P and Q are not connected by an edge of a triangle, then $D_{PQ} = 0$. Thus the matrix D is sparse.

Suppose that $P \neq Q$, and PQ is an edge belonging to two triangles, say PQR, and PQS. A classical formula from finite-element theory [16], then says that

$$D_{PQ} = -\frac{1}{2}\left\{\cot\angle R + \cot\angle S\right\}, \tag{5}$$

where $\angle R$ is the angle at the vertex R in the triangle PQR, and $\angle S$ is the angle at the vertex S in the triangle PQS.

If $P = Q$, then one has

$$D_{PP} = -\sum_{P\neq Q} D_{PQ}. \tag{6}$$

We now consider the right-hand side of (4). Recall that p is a point on the face of some triangle $\sigma = ABC$. If $Q \notin \{A, B, C\}$, then ϕ_Q is identically zero on σ and so the right-hand side of (4) is zero.

So suppose $Q \in \{A, B, C\}$, and choose the u and the v axis so that A and B are along this axis, and the positive v axis points towards C. Since ϕ_Q is linear on σ,

$$\frac{\partial\phi_Q}{\partial u} = \frac{\phi_Q(B) - \phi_Q(A)}{\|B - A\|}, \quad \frac{\partial\phi_Q}{\partial v} = \frac{\phi_Q(C) - \phi_Q(E)}{\|C - E\|},$$

where E is the orthogonal projection of C on AB.

We derive explicit formulas for E and $\phi_Q(E)$ as follows. Let θ be such that

$$E = A + \theta(B - A).$$

Since $(C - E) \perp (B - A)$, we have

$$\langle C - A - \theta(B - A), B - A\rangle = 0,$$

so

$$\theta = \frac{\langle C - A, B - A\rangle}{\|B - A\|^2}.$$

Therefore, again by the linearity of ϕ_Q on the triangle σ, we have

$$\phi_Q(E) = \phi_Q(A) + \theta(\phi_Q(B) - \phi_Q(A)).$$

If we define two real vectors $a = (a_Q) = (\frac{\partial \phi_Q}{\partial u}(p))$ and $b = (b_Q) = (\frac{\partial \phi_Q}{\partial v}(p))$, then the above formulas yield

$$a_Q - ib_Q := \begin{cases} 0 & Q \notin \{A, B, C\}, \\ \frac{-1}{\|B-A\|} + i\frac{1-\theta}{\|C-E\|} & Q = A, \\ \frac{1}{\|B-A\|} + i\frac{\theta}{\|C-E\|} & Q = B, \\ i\frac{-1}{\|C-E\|} & Q = C. \end{cases}$$

and the system (4) becomes, in matrix terms,

$$Dz = a - ib. \tag{7}$$

3.3 Solving the System of Equations

The system of linear equations (7) can be solved using standard techniques from numerical linear algebra. In practice, we solve for the real and imaginary parts of $z = x + iy$ separately, i.e. we solve $Dx = a$ and $Dy = b$.

Note that since $\sum_Q D_{PQ} = 0$ for all P, the matrix $D = (D_{PQ})$ is singular, and so we need to show that solutions to $Dx = a$ and $Dy = b$ exist. In addition, we will show that D enjoys several properties which make these solutions easy to compute numerically.

We remark that if $Dx = 0$ for some non-zero vector $x = (x_P)$, then all the elements of x are the same. To demonstrate this, suppose $Dx = 0$. Then clearly

$$\sum_{P,Q} D_{PQ} x_P x_Q = 0. \tag{8}$$

Further, by definition of the matrix D_{PQ} we have

$$\int\int_\Sigma |\nabla u|^2 dS = \sum_{P,Q} D_{PQ} x_P x_Q \tag{9}$$

where $u \in PL(\Sigma)$ is the function with $u(Q) = x_Q$ for all vertices Q. Equations (8) and (9) together imply that u is constant, and hence that all x_Q are equal. We conclude that the kernel of D is

$$H := \{\lambda(1, 1, ..., 1)^T \mid \lambda \in \mathbf{R}\}.$$

By construction, D is a sparse, real, symmetric matrix. The relation (9) implies that D is positive semi-definite, and together with the analysis above, we see that D

maps $H^\perp$, the orthogonal complement of H, bijectively to itself. Thus the equation $Dx = f$ is solvable if and only if $f \in H^\perp$ (i.e. $\sum_Q f_Q = 0$), and this solution is unique up to addition of an element of H. We note that a and b are indeed in $H^\perp$.

Since D, restricted to $H^\perp$, is sparse, symmetric and positive definite, equations $Dx = a$ and $Dy = b$ are particularly well suited for numerical solution by the well-known conjugate gradient method. Although D is singular, this method involves only multiplications by D and addition of vectors in $H^\perp$, and so quite literally solves the equations for D restricted to $H^\perp$.

The speed of the conjugate gradient method allows us to find x and y in a combined time of under 3 seconds for a surface with 8128 triangles, using a Sun UltraSparc 10.

3.4 Algorithm for Texture Mapping

We may summarize our procedure for texture mapping via the construction of a conformal map z as follows:
Input: A triangulated surface Σ, and an image to be used as a texture.

(1) Compute the elements of the matrix D, and the vectors a and b, using the formulas from section 3.2.

(2) Solve the systems of linear equations $Dx = a$ and $Dy = -b$.

(3) Compose $z = x + iy$ with inverse stereo projection to get a conformal map to the unit sphere. Specifically, send the point $x + iy$ to the point $(2x/(1 + r^2), 2y/(1 + r^2), 2r^2/(1 + r^2) - 1)$, where $r^2 = x^2 + y^2$.

(4) Compute the spherical coordinates of the points on the sphere. These will be new texture coordinates.

Output: Texture coordinates, and rendered original surface, using the new texture coordinates to index into the input image.

4 Computer Experiments

We illustrate the texture mapping procedure on a number of surfaces both synthetic and digitized.

Figures 1 through 3 are concerned with mapping textures onto synthetic surfaces which contain highly concave and convex areas. In Figure 1, we conformally map a mandrill image onto a synthetic surface. Similarly in Figure 2, we conformally map a thermal image of the earth onto a synthetic tooth-shaped surface.

Notice how in both cases the local geometry is very well-preserved, and the mappings are performed without any tears or seams in the image. Each image in Figure 3 shows two copies of the earth, one mapped to the outside and another to the inside of a vase-shaped object. The rim of the vase is not a boundary, but rather a fairly sharp edge between the inside surface of the vase and its outside. The vase is thus a topological sphere. This example demonstrates a more general property of our method; we have found it to be quite robust in the presence of edges such as those found on polyhedral surfaces.

In Figure 4, we performed a white matter segmentation of the brain whose points are colored according to mean curvature. (For details about how such a segmentation may be performed we refer the reader to [17, 23].) To get a surface triangulation, we used the Visualization Tool Kit (VTK). Using our conformal geometric technique, we then map the highly convoluted brain surface onto the sphere. Notice how the sulci (indentations) and gyri (protrusions) are clearly represented on the sphere with a nice preservation of the local geometry. Such mapping techniques have uses in functional magnetic resonance imaging for the brain flattening problem. Since it is important to visualize functional MRI data for neural activity within the folds of the brain surface, flattening methods have become an important area of research in medical imaging; see [1, 7, 23, 24] and the references therein.

Figure 5 shows how orthogonal coordinate systems, i.e. parameterizations, can be established on surfaces using our technique. The colored areas correspond to spherical rectangles with boundaries lying on lines of longitude and latitude. Notice that when these rectangles are mapped from the sphere to these surfaces, the corners of the rectangles continue to meet at right angles, due to the conformality of the mapping. As mentioned before, the conformal mapping from the surface to the sphere is not unique. Essentially, this is because we can compose the map with any conformal mapping from the sphere to itself. However, if we specify the image on the sphere of three points on the original surface, then there is only one conformal mapping which satisfies this condition. We can take advantage of this fact, because it allows us to specify which two points on the surface will correspond to the north and south poles on the sphere. In Figure 5, we have chosen these points so that the south pole is as far away as possible from the north.

Figure 6 shows how decimation of triangles affects the mapping. One-fourth of the triangles on each surface were removed to create the next surface, and the conformal mapping was re-calculated. From left to right the surfaces are composed of 32512, 8128, 2032 and 508 triangles. We made consistent choices for north and south poles on each surface so that the images could be compared visually. Removal of triangles tends to flatten out portions of the surface, and this change in geometry results in a slight shifting of the texture.

Figure 7 shows the effect of affine transformations on the procedure. The sur-

face in the upper left corner was transformed three times by multiplying its vertices by fixed matrices chosen at random. Conformal mappings to the sphere were then calculated. Again, the poles were chosen consistently to aid in visual comparison. Affine transformations alter surface angles, and so naturally the texture coordinates we calculate are not completely affine invariant. However, we note that continuously deforming the surface results in continuous changes in texture coordinates and so singularities in the texture map do not form. Here, although the differences between the surfaces are rather severe, the texture mapping remains relatively consistent. Given these results, we are very encouraged that this process may be used for automatic texture mapping. A simple example would be applying a mottled apple-skin texture to any surface that is reasonably apple-shaped.

5 Conclusions

In this section, we summarize a number of the key aspects of our method. Further, we show how the method avoids some of the problems often associated with surface mapping, and discuss applictions and areas for possible future research.

5.1 General Remarks

In this paper, we have described a general method for mapping certain surfaces to the sphere in a manner which preserves the local geometry. Since angles are preserved by this mapping, a texture, when applied to the surface, has much the same appearance that is has in the plane or on the sphere. The method also provides an effective way to establish orthogonal coordinate systems on these surfaces. Since the mapping is naturally bijective, there is no inherent problem with triangles overlapping or "flipping" when mapped to the plane. Nor does the method require cuts to be made on the surface; it is a seamless mapping and so avoids the problem of blending together textures across cuts. The formulation of the partial differential equation which is central to the method provides it with an attractive simplicity and elegance.

The simplicity of the equation formulated allows us to use standard, powerful numerical methods to solve it. The finite element method from numerical partial differential theory applied to our system with the proper boundary conditions formulated above, together with the conjugate gradient method from numerical linear algebra, form a robust and reliable solution system. As seen in the examples, this robustness shows up in the stability of the method when applied to surfaces of varying shape and triangulation, even in the presence of sharp edges. In addition, the speed of the conjugate gradient method makes the finding of the solution quite

practical.

5.2 Other Applications

We have shown how our method can be useful in automatic texture mapping, and in the construction of coordinate systems on even highly undulated surfaces. We have already discussed the application of our technique in medical imagery for functional magnetic resonance data in order to solve in a natural manner the brain flattening problem. Moreover, a number of pathologies have been associated with deformations of brain structures. We are very hopeful that our conformal methodology will be useful in quantitatively describing such pathologies.

Our conformal geometric approach can also be utilized for several other problems in computer graphics including defining the north and south poles on a given surface and in the computation of *shading maps*. Traditional computer graphics shading is done by applying synthetic lighting calculations at each polygon vertex, then interpolating between the vertices to find approximations to those values on the interior of the polygons. The cost of this calculation obviously goes up with the number of polygons. However, coarsely tesselated objects appear more realistic if shading is done at a finer scale, and finely tesselated objects are expensive to render in part because of the large number of lighting calculations. Also, it is harder to do complex shading operations in hardware where vertex-level shading is usually performed. Shading maps get around several of these problems in a number of applications. Given a mapping from 3D geometry to a 2D texture, lighting and interpolation can be performed on a regular grid in two dimensional space instead of three dimensions. Texture mapping is then used to map the result of the shading calculations back onto the surface. We plan to apply our methodology to this problem as well.

5.3 Future Research

We are currently working on the problem of global area and length distortion. It is a classical result in differential geometry (see, for example, [8]), that it is not possible to map a general surface to the sphere or plane without some distortion of lengths, and so at best a compromise must be made between length preservation and conformality of the map.

We are testing certain variational methods to find a suitable compromise between our conformal mappings and ones with minimal area and length distortions. We are also working on extending our method to surfaces with more general topology, such as surfaces with holes or boundaries.

6 Appendix: Derivation of Partial Differential Equation

In this section, we outline the derivation the partial differential equation (1). See also [1, 11, 21] and the references therein. Let p be a point on the surface Σ, $z : \Sigma \to S^2$ be a conformal equivalence which sends p to the north pole, and let (u, v) be conformal coordinates on Σ near p such that $u = v = 0$ at p. Conformal coordinates u, v are such that the metric at the point p is of the form $ds^2 = \lambda(u, v)^2(du^2 + dv^2)$. We can always ensure that at the particular point p, $\lambda(p) = 1$, $\nabla\lambda(p) = 0$. It can be proven that such conformal coordinates always exist [8]. In these coordinates, the Laplace-Beltrami operator takes the simpler, more familiar form

$$\Delta = \frac{1}{\lambda(u, v)^2}\left(\frac{\partial^2}{\partial u^2} + \frac{\partial^2}{\partial v^2}\right).$$

Set $w = u + iv$. Since the mapping $z = z(w)$ is one-to-one, it follows that z has a simple pole at $w = 0$, and hence a Laurent series representation

$$z(w) = \frac{A}{w} + B + Cw + Dw^2 + \ldots$$

We interpret this equation in the sense of distributions and apply Δ to both sides to get

$$\Delta z = A\Delta\left(\frac{1}{w}\right),$$

the non-negative powers of w being harmonic near p. We need only find z up to a constant multiple, so taking $A = \frac{1}{2\pi}$,

$$\begin{aligned}
\frac{1}{2\pi}\Delta\left(\frac{1}{w}\right) &= \frac{1}{2\pi}\Delta\left(\frac{\partial}{\partial u} - i\frac{\partial}{\partial v}\right)\log|w| \\
&= \frac{1}{2\pi}\left(\frac{\partial}{\partial u} - i\frac{\partial}{\partial v}\right)\Delta\log|w| \\
&= \frac{1}{2\pi}\left(\frac{\partial}{\partial u} - i\frac{\partial}{\partial v}\right)(2\pi\delta_p(w)),
\end{aligned}$$

where we have used the fact that $\frac{1}{2\pi}\log|w|$ is the fundamental solution for the operator Δ. This gives (1),

$$\Delta z = \left(\frac{\partial}{\partial u} - i\frac{\partial}{\partial v}\right)\delta_p.$$

Acknowledgments

We would also like to acknowledge the support of grants from NSF, AFOSR, ARO, NIH, MURI, and ONR for this research project. We would also like to thank Professor Victoria Interrante for some very helpful conversations on texture mappings.

References

[1] S. Angenent, S. Haker, A. Tannenbaum, and R. Kikinis, "Laplace-Beltrami operator and brain flattening," Technical Report, Department of Electrical and Computer Engineering, University of Minnesota, June 1998. To appear in *IEEE Trans. Medical Imaging.*

[2] C. Bennis, J.-M. Vézien, G. Iglésias, and A. Gagalowicz, "Piecewise surface flattening for non-distorted texture mapping," *Computer Graphics (SIGGRAPH '91 Proceedings)* **25**, No. 4, edited by Thomas W. Sederberg, pages 237–246, July 1991.

[3] E. A. Bier and K. R. Sloan, Jr., "Two part texture mappings," *IEEE Computer Graphics and Applications* **6**, No. 9, pages 40–53, September 1986.

[4] J. F. Blinn and M. E. Newell, "Texture and reflection in computer generated images," *Communications of the ACM* **19**, pages 542–546, 1976.

[5] J. F. Blinn, "Simulation of wrinkled surfaces," *Computer Graphics (SIGGRAPH '78 Proceedings)* **12**, No. 3, pages 286–292, August 1978.

[6] E. Catmull, *A Subdivision Algorithm for Computer Display of Curved Surfaces*, Ph. D. Thesis, Department of Computer Science, University of Utah, December 1974.

[7] C. Davatzikos and R. N. Bryan, "Using a deformable surface model to obtain a shape representation of the cortex," *IEEE Transactions on Medical Imaging* **15**, pages 785-795, 1996.

[8] M. P. Do Carmo, *Riemannian Geometry*, Prentice-Hall, Inc. New Jersey, 1992.

[9] J. Dorsey, F. Sillion, and D. Greenberg, "Design and simulation of opera lighting and projection effects," *Computer Graphics (SIGGRAPH '91 Proceedings)* **25**, No. 4, edited by Thomas W. Sederberg, pages 41–50, July 1991.

[10] M. Eck, T. DeRose, T. Duchamp, H. Hoppe, M. Lounsbery, and W. Stuetzle. "Multiresolution analysis of arbitrary meshes," *Computer Graphics (SIGGRAPH '95 Proceedings)* **29**, pages 173-182, 1995.

[11] H. Farkas and I. Kra, *Riemann Surfaces,* Springer-Verlag, New York 1991.

[12] J. Foley, A. van Dam, S. Feiner, and J. Hughes, *Computer Graphics,* Addison-Wesley Publishing, Massachusetts, 1992.

[13] J. Gomes, L. Darsa, B. Costa, and L. Velho, *Warping & Morphing of Graphical Objects,* Morgan Kaufman Publishers, 1998.

[14] P. S. Heckbert, "Survey of texture mapping," *IEEE Computer Graphics and Applications* **6**, No. 11, pages 56–67, November 1986.

[15] P. S. Heckbert, *Fundamentals of Texture Mapping and Image Warping,* Masters Thesis, Department of Electrical Engineering and Computer Science, University of California, Berkeley, June 1989.

[16] T. Hughes, *The Finite Element Method,* Prentice-Hall, New Jersey, 1987.

[17] S. Kichenasamy, A. Kumar, P. Olver, A. Tannenbaum, A. Yezzi, "Conformal curvature flows: from phase transitions to active contours," *Archive Rational Mechanics and Analysis* **134**, pages 275-301, 1996.

[18] A. W. F. Lee, W. Sweldens, P. Schröder, L. Cowsar, and D. Dobkin, "MAPS: multiresolution adaptive parameterization of surfaces," *Computer Graphics (SIGGRAPH '98 Proceedings)* **32**, edited by Michael Cohen, Addison-Wesley Publishing Company, pages 95–104, July 1998.

[19] B. Lévy and J. L. Mallet, "Non-distorted texture mapping for sheared triangulated meshes," *Computer Graphics (SIGGRAPH '98 Proceedings)* **32**, edited by Michael Cohen, Addison-Wesley Publishing Company, pages 343–352, July 1998.

[20] T. McReynolds, "Advanced graphics programming techniques using OpenGL," *SIGGRAPH '98 Course Notes,* pages 90–99, 1998.

[21] J. Rauch, *Partial Differential Equations,* Springer-Verlag, New York 1991.

[22] M. Segal, C. Korobkin, R. van Widenfelt, J. Foran, and P. E. Haeberli, "Fast shadows and lighting effects using texture mapping," *Computer Graphics (SIGGRAPH '92 Proceedings)* **26**, edited by Edwin E. Catmull, pages 249–252, July 1992.

[23] P. Teo, G. Sapiro, and B. A. Wandell, "Creating connected representations of cortical gray matter for functional MRI visualization," *IEEE Transactions on Medical Imaging* **17**, 1998.

[24] B. Wandell, S. Engel, and H. Hel-Or, "Creating images of the flattened cortical sheet," *Invest. Opth. and Vis. Sci.* **36** (S612), 1996.

[25] A. Watt and M. Watt, *Advanced Animation and Rendering Techniques: Theory and Practice,* Addison-Wesley Publishing Company, New York, 1992.

Figure 1: Mandrill Image on Synthetic Surface

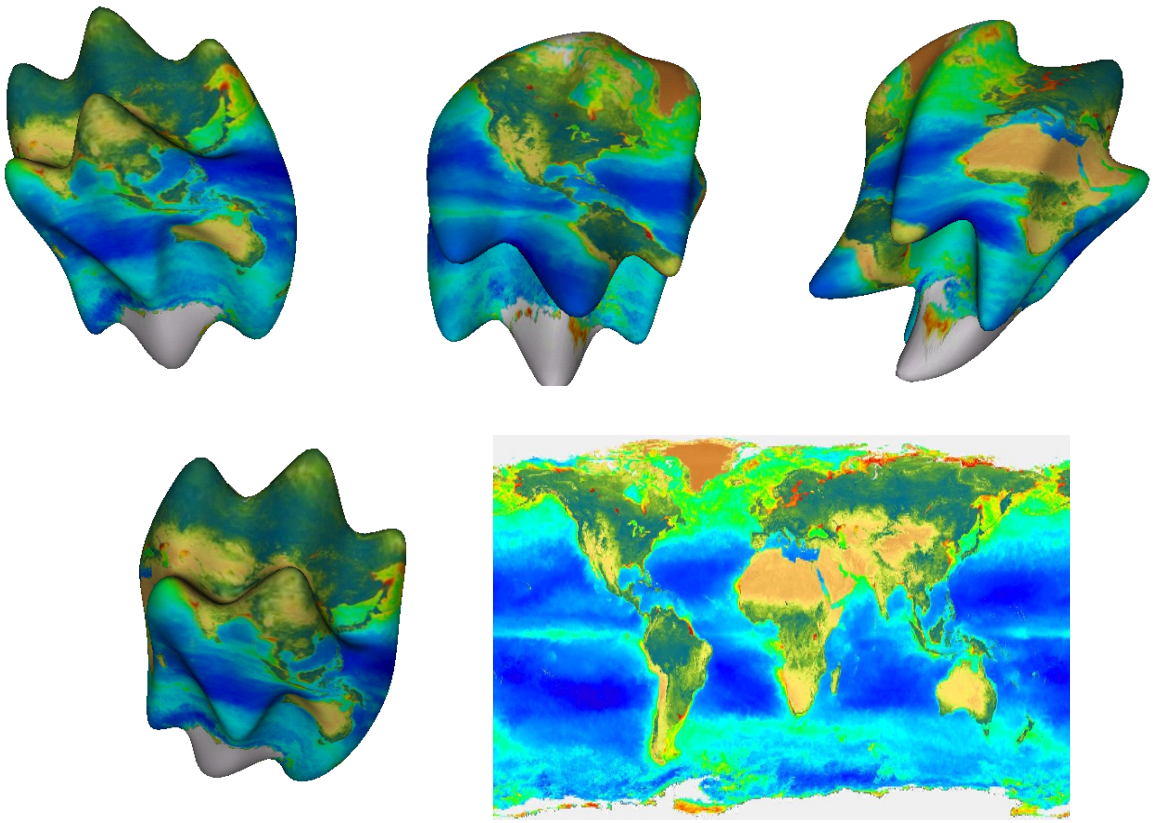

Figure 2: Thermal Image of Earth on Synthetic Surface

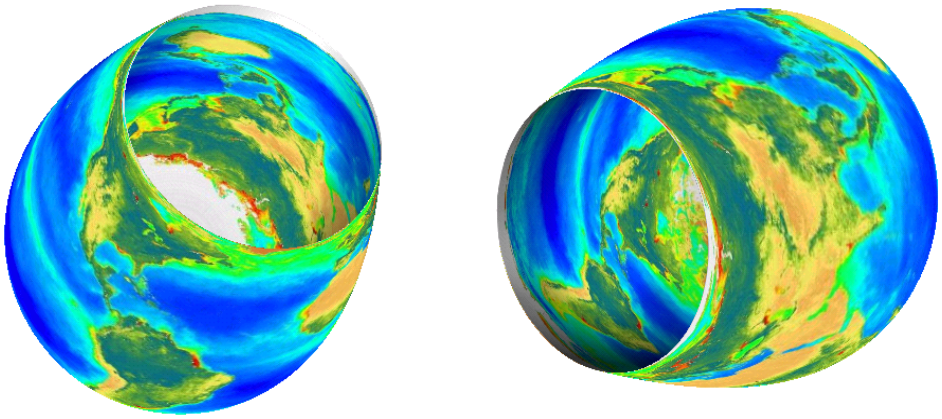

Figure 3: Earth on Inside and Outside of a Vase

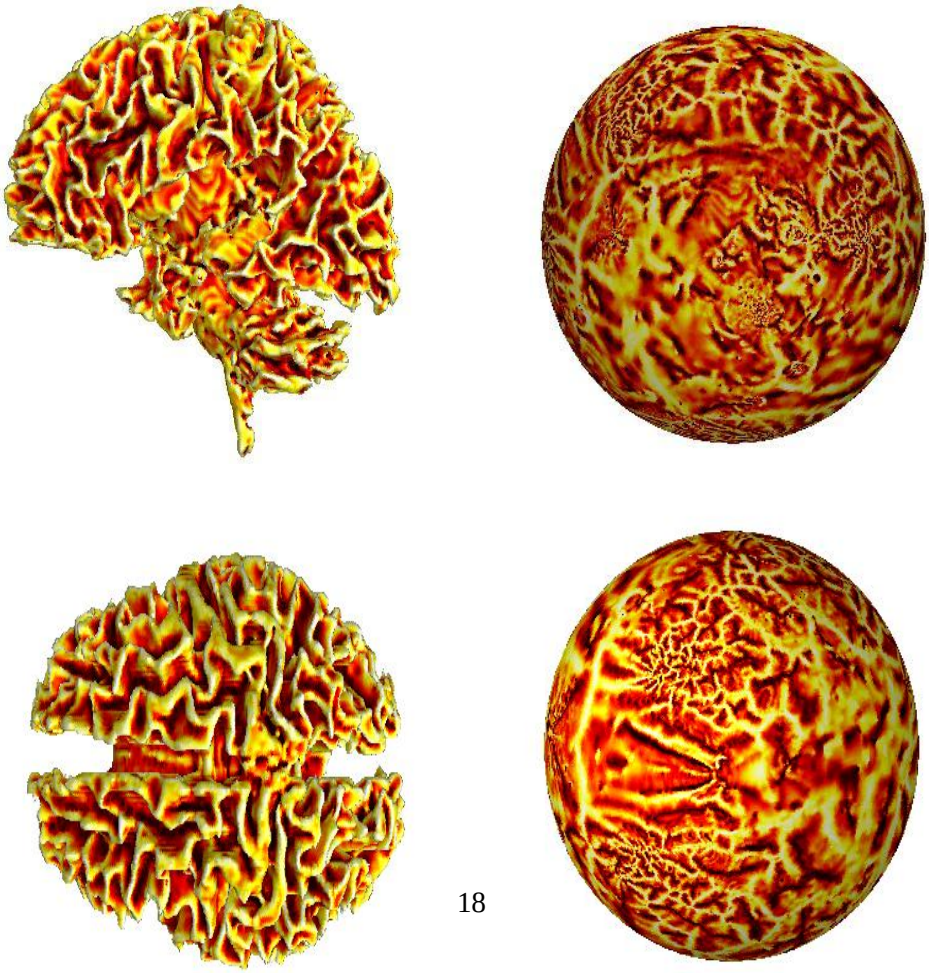

Figure 4: Two Views of Flattened White Matter

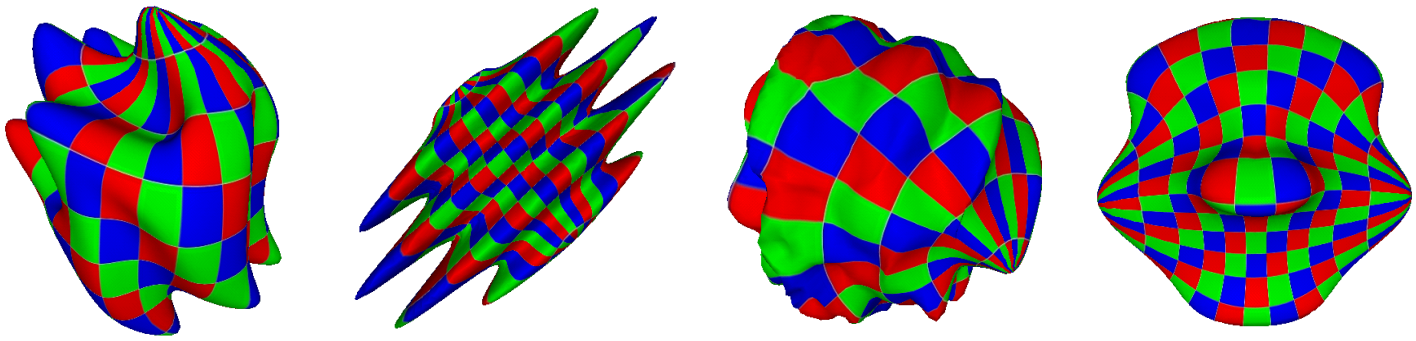

Figure 5: Orthogonal Coordinate Systems

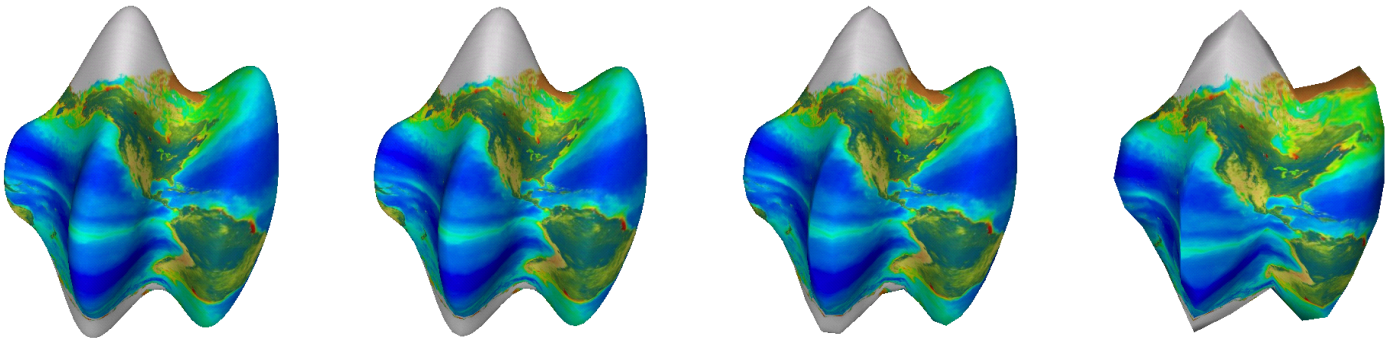

Figure 6: Effect of Triangle Decimation

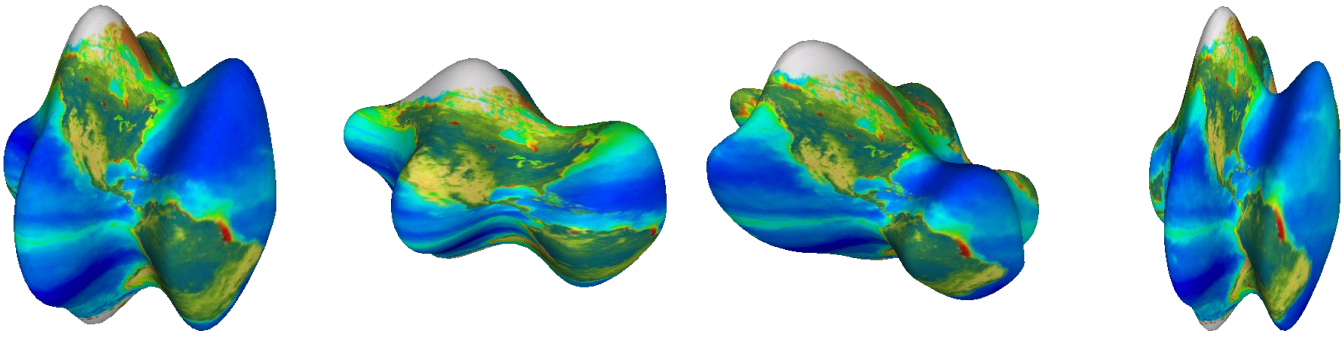

Figure 7: Effect of Affine Transformations